Rotordynamics and Vibration Analysis Tool for Engine Driveline Testrig Facility at Aberdeen Proving Ground

Final Report

PRINCIPLE INVESTIGATOR:
Dr. Hans DeSmidt, Ph.D.
Professor of Aerospace Engineering
234 Dougherty Bldg
University of Tennessee
Knoxville, TN 37996
Phone: 865-406-9967
Email: hdesmidt@utk.edu

CONTRACT NO: W911NF2020193

CONTRACTOR NAME AND ADDRESS:
UNIVERSITY OF TENNESSEE
UNIV TENNESSEE SYSTEM OFFICE
1331 CIR PARK DR

DATE PREPARED: 11 OCT 2022

PERIOD OF PERFORMANCE: July 2020 - July 2022
TOTAL BUDGET: $132,885.00

REPORT DOCUMENTATION PAGE

Form Approved
OMB No. 0704-0188

1. REPORT DATE *(DD-MM-YYYY)*	2. REPORT TYPE	3. DATES COVERED *(From - To)*
10-11-2022	Final Technical Report	24-07-2020-23-07-2022

4. TITLE AND SUBTITLE
Rotordynamics & Vibration Analysis Tool for Engine Driveline Testrig Facility at Aberdeen Proving Ground

5a. CONTRACT NUMBER
W911NF-20-2-0193

5b. GRANT NUMBER
n/a

5c. PROGRAM ELEMENT NUMBER
n/a

6. AUTHOR(S)
Dr. Hans DeSmidt, Ph.D.

5d. PROJECT NUMBER
n/a

5e. TASK NUMBER
n/a

5f. WORK UNIT NUMBER
n/a

7. PERFORMING ORGANIZATION NAME(S) AND ADDRESS(ES)
UNIVERSITY OF TENNESSEE
UNIV TENNESSEE SYSTEM OFFICE
1331 CIR PARK DR
KNOXVILLE TN 37916-3801

8. PERFORMING ORGANIZATION REPORT NUMBER
A21-0216

9. SPONSORING/MONITORING AGENCY NAME(S) AND ADDRESS(ES)
US ARMY ACC-APG-RTP W911NF
800 PARK OFFICE DRIVE, SUITE 4229
RESEARCH TRIANGLE PARK NC 27709

10. SPONSOR/MONITOR'S ACRONYM(S)
ACC-APG-RTP

11. SPONSOR/MONITOR'S REPORT NUMBER(S)
n/a

12. DISTRIBUTION/AVAILABILITY STATEMENT
Open publication policy

13. SUPPLEMENTARY NOTES

14. ABSTRACT

The overall goal of this proposed project has been to develop rotordynamics and vibration models for the Small Engine Altitude Research Facility (SmEARF) and the Small Engine Combustion Research Laboratory (SECRL) at Aberdeen Proving Ground (APG) in the U.S. Army Combat Capabilities Development Command (DEVCOM) Army Research Laboratory (ARL). These models enable prediction of critical speeds, vibration modeshapes and assist with driveline component and engine-mount selection to avoid vibration over the engine test speed ranges.

15. SUBJECT TERMS
Small Engine Altitude Research Facility (SmEARF)
Small Engine Combustion Research Laboratory (SECRL)
Finite Element Model (FEM)

16. SECURITY CLASSIFICATION OF:			17. LIMITATION OF ABSTRACT	18. NUMBER OF PAGES	19a. NAME OF RESPONSIBLE PERSON
a. REPORT	b. ABSTRACT	c. THIS PAGE			Stephanie C. Jonas-Fields
n/a	n/a	n/a	SAR	16	19b. TELEPHONE NUMBER *(Include area code)* 865-974-8795

1. Introduction and Motivation:

The overall goal of this proposed project has been to develop rotordynamics and vibration models for the Small Engine Altitude Research Facility (SmEARF) and the Small Engine Combustion Research Laboratory (SECRL) at Aberdeen Proving Ground (APG) in the U.S. Army Combat Capabilities Development Command (DEVCOM) Army Research Laboratory (ARL). These models enable prediction of critical speeds, vibration modeshapes and assist with driveline component and engine-mount selection to avoid vibration over the engine test speed ranges.

2. Rotordynamics Finite Element Modeling

The PI has developed a Finite Element Model (FEM) rotordynamics modeling code in Matlab® to analyze, torsion and lateral vibration modes and critical speeds (RPM) of a general engine driveline dynamometer system which was then adapted to model the specific engine testrig configurations. Figure 1 shows a photo and schematic of the ARL/APG Small Engine Altitude Research Facility (SmEARF) drivesystem along with some of the components included in the analysis.

(a)

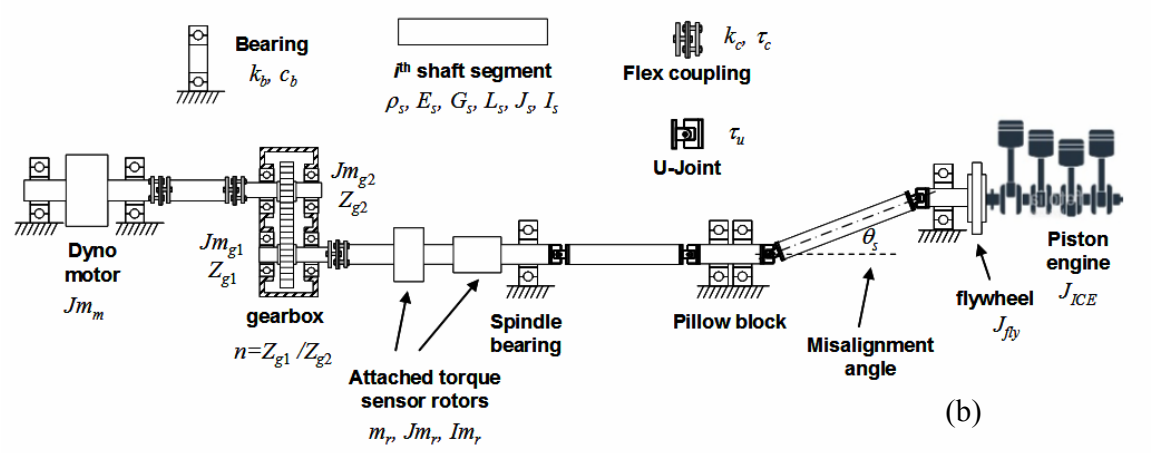

(b)

Fig. 1, ARL/APG Small Engine Altitude Research Facility (SmEARF) drivesystem

The driveshaft segments are modeled as rotating Euler-Bernoulli beams with bending and torsional flexibility, gyroscopic effects, and rotating-frame damping. Figure 2 shows a schematic of the flexible shaft rotordynamics model. The support bearings and flexible couplings are modeled as linear and torsional springs respectively. In order to accurately capture effects of

multiple shaft segments joined by flexible couplings with various bearing supports, boundary conditions and attached inertias such as torque sensor rotors, the driveline system model were formulated using a Finite Element Method (FEM) approach as depicted in fig. 3.

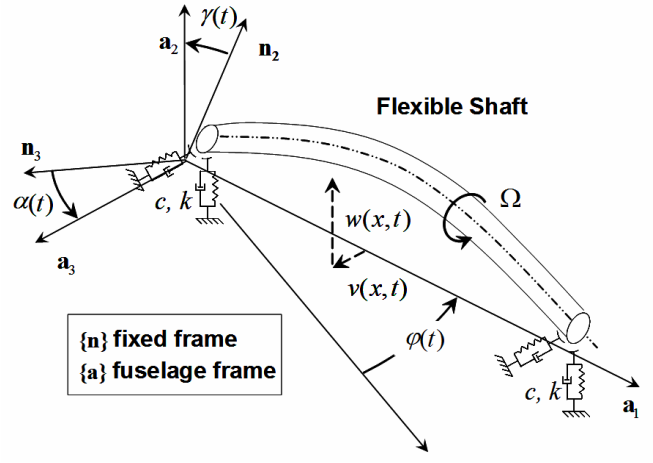

Fig. 2, flexible shaft rotordynamics model

Each shaft segment was discreteized into N_{el}^{i} beam-rod-torsion elements each with element length $L_{el}^{i} = L_i / N_{el}^{i}$ and two 6-degree-of-freedom (DOF) nodes. Equation (1) shows the corresponding nodal and elemental displacement DOF.

$$q_{node,j}^{i} = [v_{i,j}\ \theta_{3i,j}\ w_{i,j}\ \theta_{2i,j}\ u_{i,j}\ \theta_{1i,j}]^T \quad \text{and} \quad q_{el,j}^{i} = \begin{bmatrix} q_{node,j}^{i} \\ q_{node,j+1}^{i} \end{bmatrix} \tag{1}$$

Furthermore, the shaft elemental inertia matrix, $\mathbf{M}_{el,j}^{i}$, gyroscopic matrix $\mathbf{G}_{el,j}^{i}$, damping matrix $\mathbf{C}_{el,j}^{i}$ and elastic stiffness matrix $\mathbf{K}_{el,j}^{i}$ have the form [1]

$$\begin{aligned}
\mathbf{M}_{el,j}^{i} &= \int_0^{L_{el}^{i}} \left[m_s (N_u^T N_u + N_v^T N_v + N_w^T N_w) + Im_s (N_v'^T N_v' + N_w'^T N_w') + Jm_s N_\phi^T N_\phi \right] dx \\
\mathbf{G}_{el,j}^{i} &= \int_0^{L_{el}^{i}} Jm_s \Omega_i (N_v'^T N_w' - N_w'^T N_v') dx \\
\mathbf{C}_{el,j}^{i} &= \xi_s \int_0^{L_{el}^{i}} \left[E_s A_s N_u'^T N_u' + E_s I_s (N_v''^T N_v'' + N_w''^T N_w'') + G_s J_s N_\phi'^T N_\phi' \right] dx \\
\mathbf{K}_{el,j}^{i} &= \int_0^{L_{el}^{i}} \left[E_s A_s N_u'^T N_u' + E_s I_s \left(N_v''^T N_v'' + N_w''^T N_w'' \right) + G_s J_s N_\phi'^T N_\phi' \right] dx
\end{aligned} \tag{2}$$

After model assembly, boundary constraint application and including the effect of a small rotational imbalance, the rotordynamic equations of the driveline system will have the form

$$\mathbf{M}\ddot{q} + \left[\mathbf{C} + \mathbf{G}(\Omega_0)\right]\dot{q} + \left[\mathbf{K} + \mathbf{K}_{rd}(\Omega_0)\right]q = \mathbf{Q}_{\mathbf{imb}} \begin{bmatrix} \cos(\Omega_0 t) \\ \sin(\Omega_0 t) \end{bmatrix} \tag{3}$$

Due to the gyroscopic effects and rotating frame damping terms in (3), the system modal characteristics will inherently be a function of the shaft operating speed Ω_0.

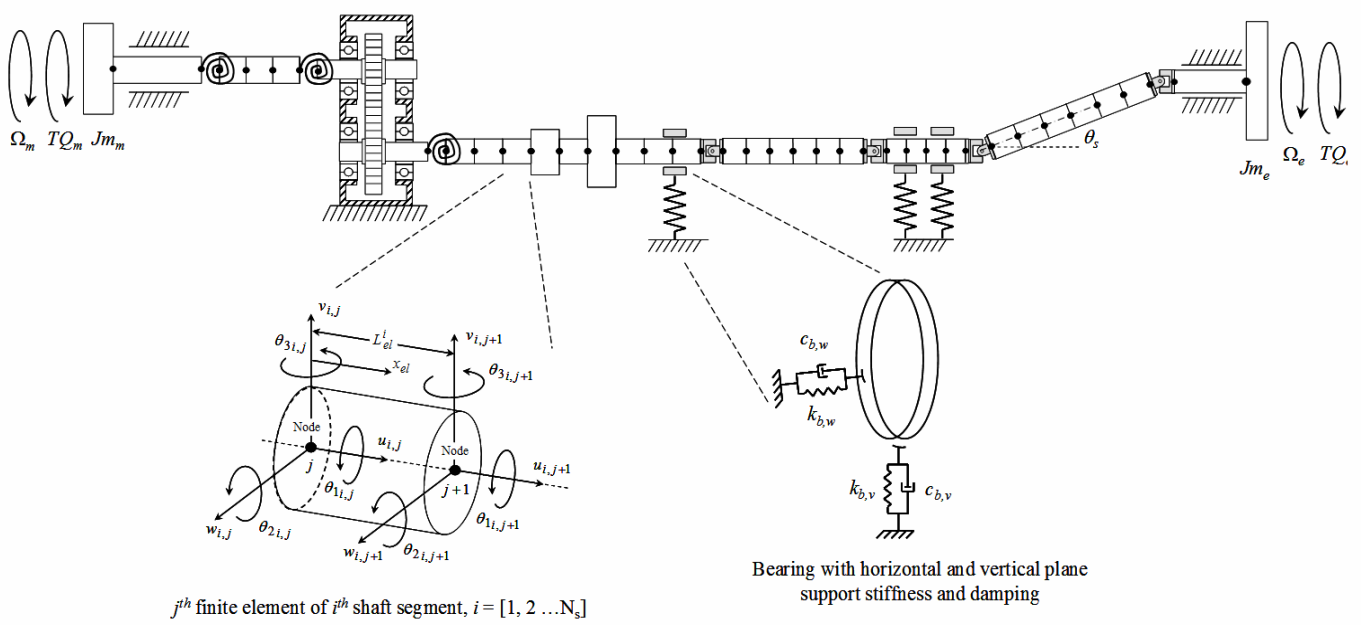

Fig. 3 Finite Element Model formulation of APG Engine Altitude Research Facility (SmEARF) divesystem

Furthermore, fig 4 shows a photo of the SECRL testrig and fig. 5 shows a schematic of the associated rotordynamics model developed under this project. One main feature of the SECRL testrig is the relatively long span of unsupported shaft between left side dynamometer and right side engine mounts. In this arrangement the engine block and associated engine mount compliance become important parts of the overall lateral dynamics of the drivesystem. To account for this in the rotordynamics model, the engine block is considered as a 6 DOF (axial, horizontal, vertical plunging and yaw, pitch and roll) lumped inertia mounted on a four springs that model engine mount compliance (see fig 5).

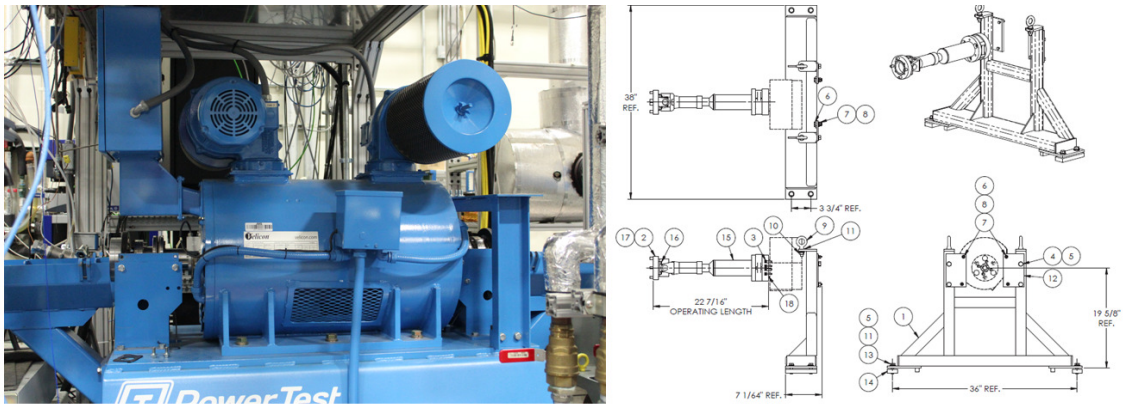

Fig. 4, SECRL testrig photo and engine stand diagram

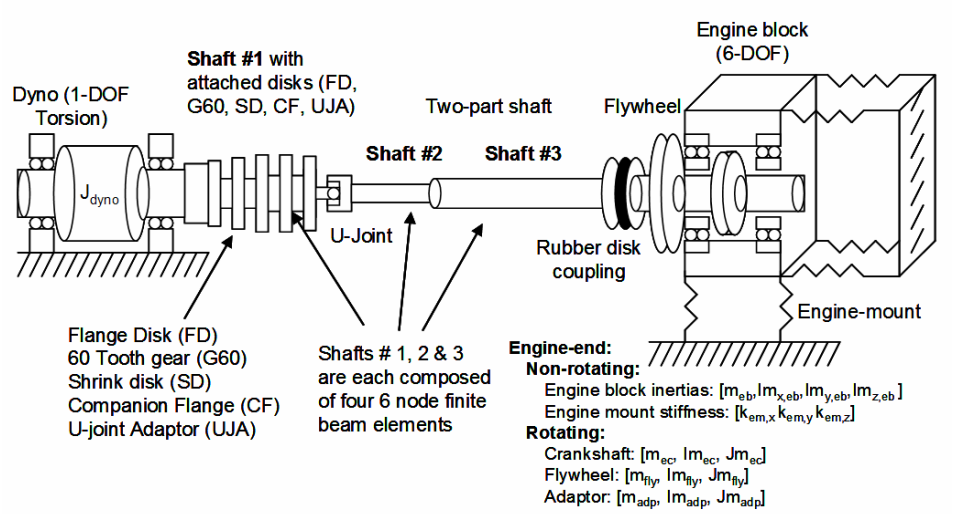

Fig. 5, SECRL testrig rotordynamics model including engine mount compliance and 6 engine block DOF

Engine block dynamics due to compliant elastomertic type engine mounts also played an important role in several of the SmEARF testrig setups. Therefore a similar approach to model the 6 engine DOF was also employed in these cases as well.

In the driveline a variety of couplings such as universal joints (U-joints), flange couplings, disk/diaphragm couplings and elastomeric couplings are utilized to connect various shaft segments. Each type of coupling has different stiffness and kinematic characteristics which were accounted for in the rotordynamic models. In the driveline FEM, the couplings are modeled as lumped spring stiffnesses which link adjacent shaft segment nodal DOF. In order to estimate the effective torsional k_t, axial, k_a, radial, k_r and angular k_θ stiffness values, a variety of methods were utilized. In the case of disk and flange couplings, a 3-D static finite element analysis (FEA) utilizing Ansys® was preformed to determine the stiffness values based on a unit load analysis as depicted in figure 6.

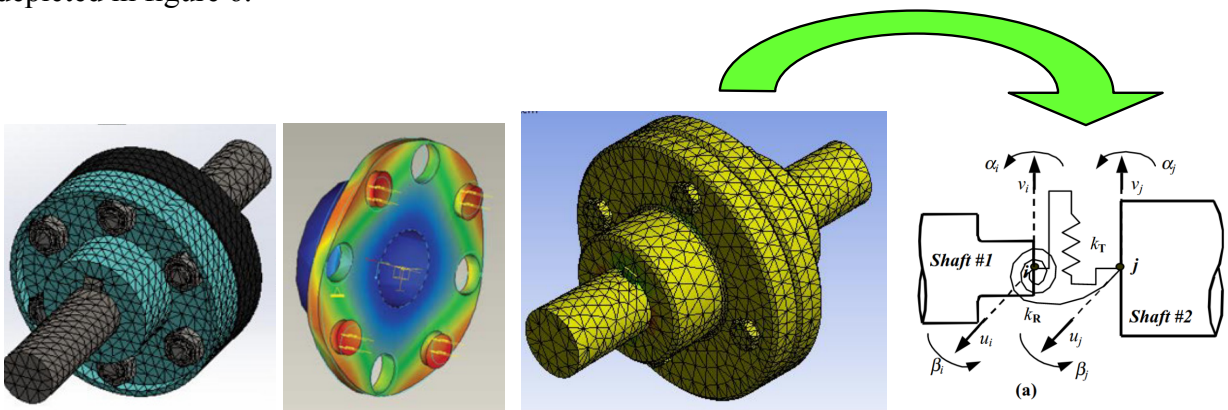

Fig. 6 Flange coupling lumped parameter 6-DOF stiffness distillation from 3D static FEA

Also, as shown in (fig. 7) both the SmEARF and SECRL testrigs involve universal joint couplings (U-Joints) to accommodate center position differences between engine and driveline. Due to the kinematics of U-joint couplings, whenever misalignment exists small speed fluctuations about the nominal input speed will occur within each shaft segment depending on the misalignment configuration. Figure 8 shows an example of these speed fluctuations for various driveline misalignment conditions in a multi-segment driveline connected by U-joints. These misalignment induced speed fluctuations produce multiple harmonic torsional and lateral excitations at $N\ x\ \Omega_0$ frequencies as mentioned previously. The driveline misalignment effects will be is accounted for in the testrig rotordynamics models by including the flexible coupling kinematics within the dynamics model

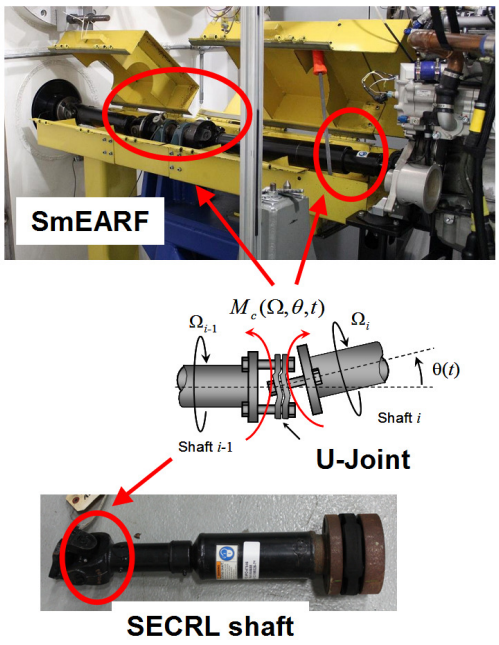

Fig. 7, Universal joint couplings utilized in the SmEARF and SECRL driveshafts to accommodate angular misalignments

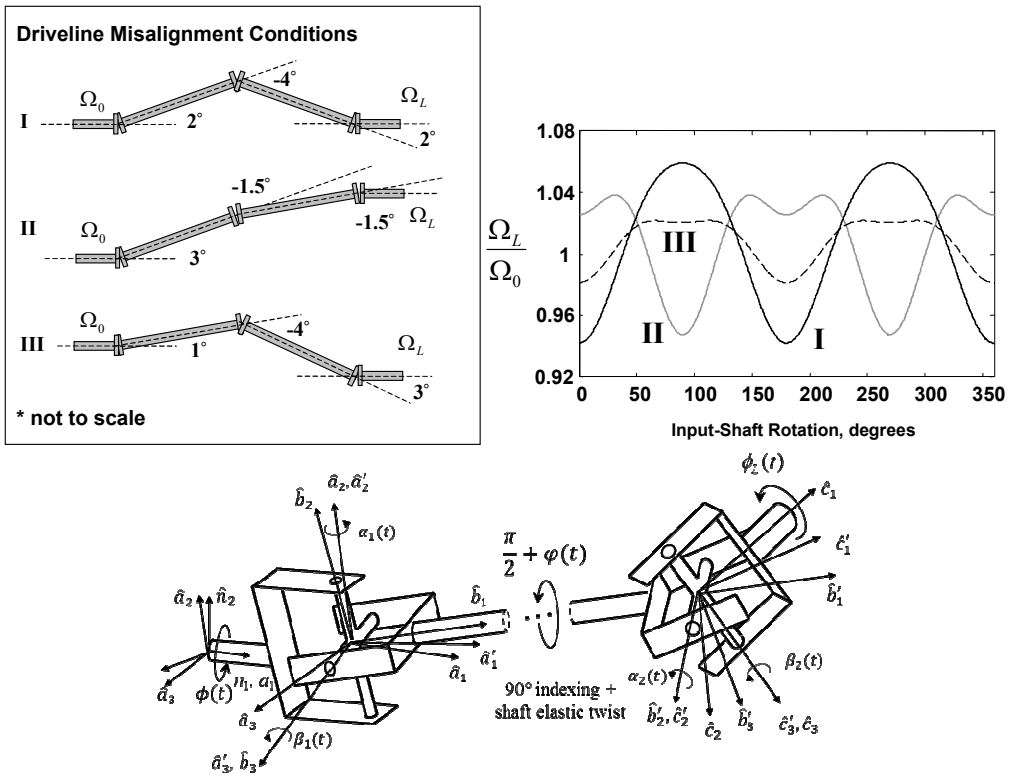

Fig. 8, Misalignment induced driveshaft speed fluctuations.

Equation 4 shows the functional relationship between the shaft speed of the i^{th} segment, Ω_i, and i^{th}+1 segment Ω_{i+1}.

$$\Omega_{i+1} = \Omega_i + f_0(\Omega_0, \theta_i, \dot{\theta}_i) + f_c(\Omega_0, \theta_i, \dot{\theta}_i)\cos 2\Omega_0 t + f_s(\Omega_0, \theta_i, \dot{\theta}_i)\sin 2\Omega_0 t \tag{4}$$

where θ_i and $\dot{\theta}_i$ are misalignment angle and misalignment angle rate respectively between the i^{th} and i^{th}+1 shaft segments. When rotational imbalance and misalignment are included, the resulting driveline equations of motion will have the following form [2]

$$\begin{aligned}\left[\mathbf{M}_0 + \mathbf{M}_s \sin 2\Omega_0 t + \mathbf{M}_c \cos 2\Omega_0 t\right]\ddot{q} + \left[\mathbf{C} + \mathbf{G}(\Omega_0)\right]\dot{q} + \left[\mathbf{K} + \mathbf{K}_{rd}(\Omega_0)\right]q \\ \ldots = \mathbf{F}_{imb}\begin{bmatrix}\cos(\Omega_0 t)\\ \sin(\Omega_0 t)\end{bmatrix} + \mathbf{F}_0 + \sum_{n=}^{N}(\mathbf{F}_{s,n}\sin 2n\Omega_0 t + \mathbf{F}_{c,n}\cos 2n\Omega_0 t)\end{aligned} \tag{5}$$

Here, angular misalignment produces the periodically time varying inertia matrix terms, $\mathbf{M}_s$ and $\mathbf{M}_c$, as well as multiple harmonic excitation terms $\mathbf{F}_0$, $\mathbf{F}_{s,n}$ and $\mathbf{F}_{c,n}$. Furthermore, the rotational imbalance produces the synchronous excitation term $\mathbf{F}_{imb}$.

Yet another type of coupling frequently utilized in the ARL/APG testrigs are elastomeric couplings with various geometries. One example is the shaft shown in fig. 9 which is equipped with dual elastomeric torsional isolators.

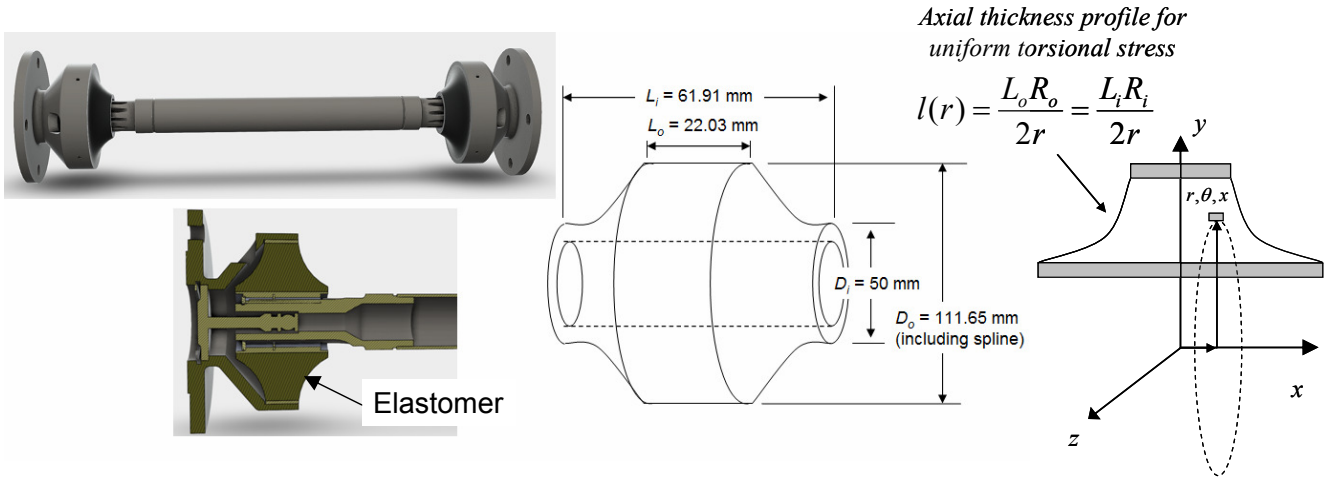

Fig. 9, Shaft with elastomeric bushing-type torsional isolator couplings

The stiffness values of this shaft coupling were determined via an energy method approach, in this case using Castigliano's 2nd theorem. The resulting expressions for torsional and radial stiffness are

$$k_t = G\frac{2\pi L_o R_o^{\,2}}{\ln(R_o/R_i)}, \quad k_r = \frac{2\pi\, EL_o}{\ln(R_o/R_i) - 2(R_o^{\,2} - R_i^{\,2})/R_o^{\,2}}, \quad \text{and} \quad k_\theta = \frac{k_r L^2}{12} \tag{8}$$

where E and G are the elastic and shear moduli of the rubber isolator material and R_o, R_i and L_o are the outer radius, inner radius and length of the isolator. The other type of elastomeric coupling modeled are flex-disk or "giubo" couplings (see fig. 10).

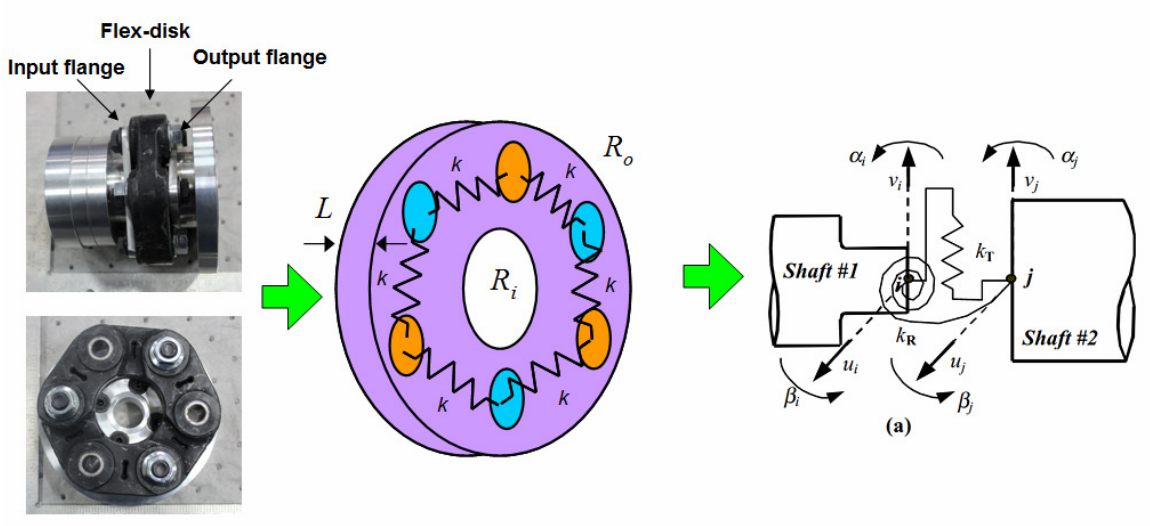

Fig. 10, Flex-disk and giubo shaft couplings

To estimate the system stiffness, the elstomeric disk is approximated as a set of 6 linear springs which link the 3 rigid pins on the input flange to the 3 pins on the output flange as shown in figure 10. After applying Castigliano's theorem, the coupling stiffness expressions are obtained

$$k_t = \frac{27}{4\pi} E(R_o^{\,2} - R_i^{\,2})L \quad \text{and} \quad k_r = E\frac{18}{\pi}\frac{R_o - R_i}{R_o + R_i}L \tag{7-a}$$

$$k_\theta = E\frac{\pi}{8L}(R_o^{\,4} - R_i^{\,4}) \quad \text{and} \quad k_a = E\frac{\pi(R_o^{\,2} - R_i^{\,2})}{L} \tag{7-b}$$

Finally, several stiffness models for engine mounts have been developed and utilized in this work. The first type of engine mount is a cylindrical bushing which is depicted in fig 11.

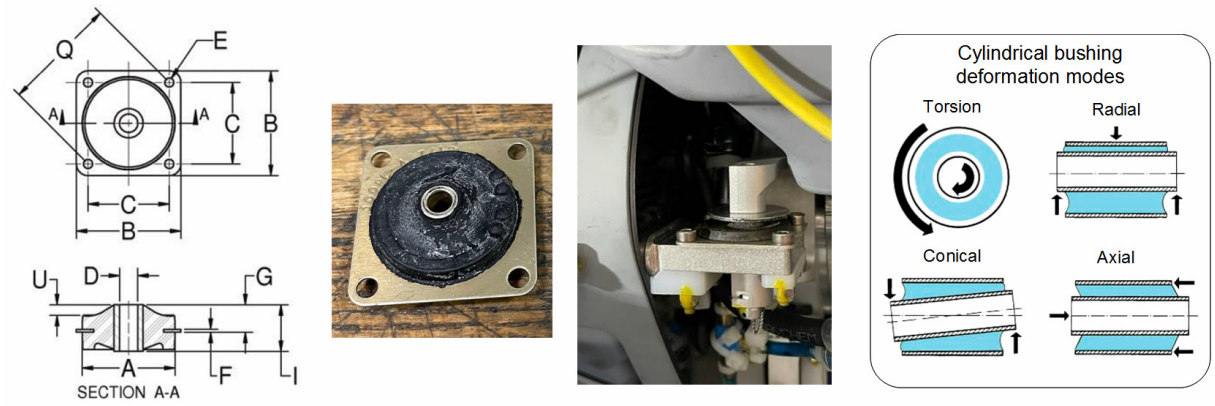

Fig. 11, Cylindrical bushing elastomeric engine mount

The derived stiffness expressions for engine mount bushings are

$$k_t = G\frac{4\pi L R_o^{\,2} R_i^{\,2}}{R_o^{\,2} - R_i^{\,2}}, \text{ and } \quad k_r = \frac{2\pi\, EL}{\ln(R_o / R_i) - 2(R_o^{\,2} - R_i^{\,2})/R_o^{\,2}} \tag{9-a}$$

$$k_\theta = \frac{k_r L^2}{12}, \quad \text{and} \quad k_a = G\frac{2\pi L^3}{L^2 \ln(R_o / R_i) + \frac{3}{8}\frac{(R_o^{\,2}\text{-}R_i^{\,2})^2 - 4R_o^{\,2}R_i^{\,2}\log(R_o / R_i)^2}{R_o^{\,2} - R_i^{\,2}}} \tag{9-b}$$

The other typ of mount is the so-called vibration dampening sandwich stud mount shown in fig. 12. The stiffness of the mount was derived by treating it as a short cantilever short cantilever beam loaded at the tip.

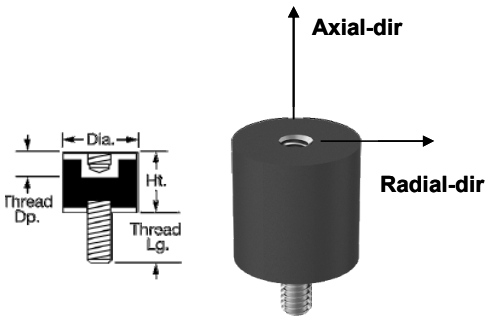

Fig. 12, Vibration dampening sandwich stud mount

Here, bending, transverse shear, torsion and axial stresses were all included. The resulting mount stiffness relations represented in matrix form are given in equation 10.

$$\begin{bmatrix} F_y \\ M_z \\ F_z \\ M_y \\ F_x \\ M_x \end{bmatrix} = \begin{bmatrix} k_r & -k_{r\theta} & 0 & 0 & 0 & 0 \\ -k_{r\theta} & k_\theta & 0 & 0 & 0 & 0 \\ 0 & 0 & k_r & k_{r\theta} & 0 & 0 \\ 0 & 0 & k_{r\theta} & k_\theta & 0 & 0 \\ 0 & 0 & 0 & 0 & k_a & 0 \\ 0 & 0 & 0 & 0 & 0 & k_t \end{bmatrix} \begin{bmatrix} v \\ \theta_z \\ w \\ \theta_y \\ u \\ \phi \end{bmatrix} \tag{10-a}$$

with

$$k_r = \frac{1}{\frac{L^3}{12EI} + \frac{f_s L}{GA}}, \; k_{r\theta} = \frac{1}{\frac{L^2}{6EI} + \frac{2f_s}{GA}}, \quad k_\theta = \frac{4EI}{L}\frac{3EIf_s + GAL^2}{12EIf_s + GAL^2} \tag{10-b}$$

and

$$k_a = \frac{EA}{L} \quad \text{and} \quad k_t = \frac{GJ}{L} \tag{10-c}$$

Utilizing the system matrices from the FEM code, the modeshapes and natural frequencies are computed via the state-space approach which includes the effects of mass, damping, gyroscopic and stiffness terms.

$$\dot{\mathbf{x}} = \begin{bmatrix} \dot{q} \\ \ddot{q} \end{bmatrix} = \begin{bmatrix} \mathbf{0} & \mathbf{I} \\ -\mathbf{M}^{-1}(\mathbf{K} + \mathbf{K}_{rd}(\Omega_0)) & -\mathbf{M}^{-1}(\mathbf{C} + \mathbf{G}(\Omega_0)) \end{bmatrix} \begin{bmatrix} q \\ \dot{q} \end{bmatrix} = \mathbf{A}(\Omega_0)\mathbf{x} \qquad (11\text{-a})$$

$$\mathbf{x}(t) = \mathbf{u}e^{\lambda t}, \qquad \mathbf{A}\mathbf{u}_i = \lambda_i \mathbf{u}_i, \qquad \lambda_i = \alpha_i \pm j\omega_i \qquad (11\text{-b})$$

Since the driveline natural frequencies are speed dependent, the driveline critical speeds are determined by evaluating the intersections of the operating speed line with the natural frequencies over the range of operating speeds Ω_0. In addition the engine order excitations based on piston firing and crank angle are also evaluated

3. Analysis Results

The rotordynamic analysis model was configured to analyze critical speeds and vibration for multiple engine test setups on both the SmEARF and SECRL facilities. In order to calibrate the FEM model, lab personnel at APG performed several modal vibration tests on the non-rotating SmEARF with a single cylinder 4 hp engine installed (see fig. 13). Here a modal impact hammer was used to excite the driveline by striking it at several locations near the pillow block and the engine block with the engine off (zero engine RPM). Data from accelerometers located on the engine block and pillow block bearing was then utilized to generate the vibration frequency responses of the driveline.

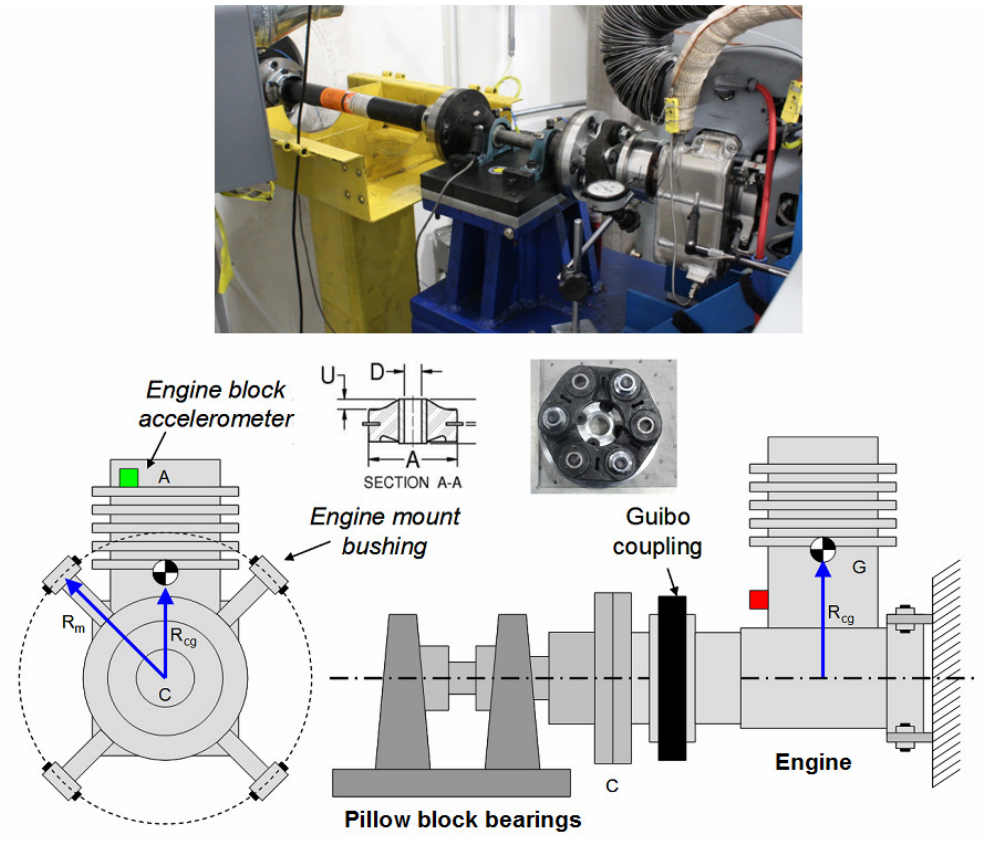

Fig. 13, SmEARF with 4 Hp single cylinder engine installed

Figure 14 shows as schematic representation of the rotordynamics FEM code configured for the SmEARF system. Here the model consists of 7 individual shaft segments starting at the dynamometer-end as well as the engine block DOF as described in the previous section of this report.

```
% SmEARF, 4Hp Engine                                                                                                  [---------]
% Dyno / Driveline / Engine                                                                                            [         ]
%                                                                                                                      [ mBLOCK  ]      /
%               {n2} y-dir                                                                                             [   G   B1]/\/\//
%                 |                                                                                                    [         ]     /
%                 |      b1,b2  b3,b4            b5       b6                 b7  b8                  b9 b10          [         ]    /
%                 |                                                                                                    [------]  ]
%  ///        /// |        //  //               //      //                // //                      // //      fly   o    o   ]
%  oo [-----] oo []     [] oo  oo []          [] o  [--]  o []           [] o   o []              [] [] o  o [] [] [-] [--------] ]
% ----[JDYNO]---[  ]---[  ]------[  ]--------[  ]---[  ]---[  ]---------[  ]-----[  ]-----------[  ][]------[][  ][ ]-[ JCRANK ] ]--> n1
%  oo [-----] oo []     [] oo  oo []          [] o  [--]  o []           [] o   o []              [] [] o  o [] [] [-] [--------] ]    x
% ///        /// c1     c2 //  // c3          c4 // JTQT // c5           c6 // // c7              c8   // //    c9       o    o   ]
%                                                                                                                      [------]  ]     /
%                  XHD      GBX       shft2        TQT          shft3      spindle     shft4          PB             [       B2]/\/\//
%   FEM Shaft#      1        2         3            4            5          6           7              8              [---------]     /
%
%
```

Fig. 14, Rotordynamics FEM code configured for SmEARF / 4 Hp engine system analysis

Figure 15 shows a comparison between the experimentally generated and analytically computed vibration frequency response from the rotordynamics FEM code for the SmEARF/ 4 Hp engine system.

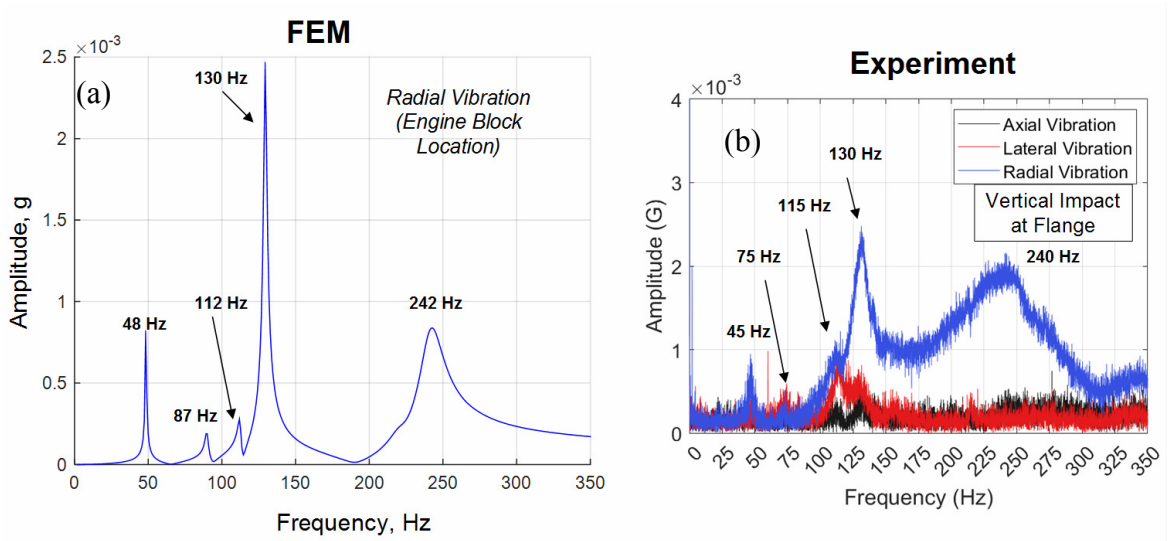

Fig. 15, Vibration frequency response comparison between rotordynamics FEM code and experimental data for SmEARF / 4 Hp engine system (engine speed 0 RPM)

The results of the frequency response comparison shows that the FEM code is in good agreement with experimental data. In particular, the location of the system natural frequencies as well as the response magnitudes are well matching. Furthermore, fig. 16 shows the results of a parameter sensitivity analysis which was conducted by independently varying the engine mount stiffness (fig. 16-a), the shaft flex-disk coupling stiffness (fig. 16-b) and the pillow block bearing support stiffness (fig. 16-c). This analysis shows that the 1st mode around 50 Hz mainly involves the pitching motion of the engine block with the modes around 130 and 240 Hz are primarily shaft modes with little or no engine block involvement. This is further shown in fig 17 which demonstrates how the modeshapes are affected by the engine mount stiffness. figure 17-b shows

that some natural frequencies increase with the engine mount stiffness (engine block/shaft coupled modes) while other modes are insensitive (pure shaft modes).

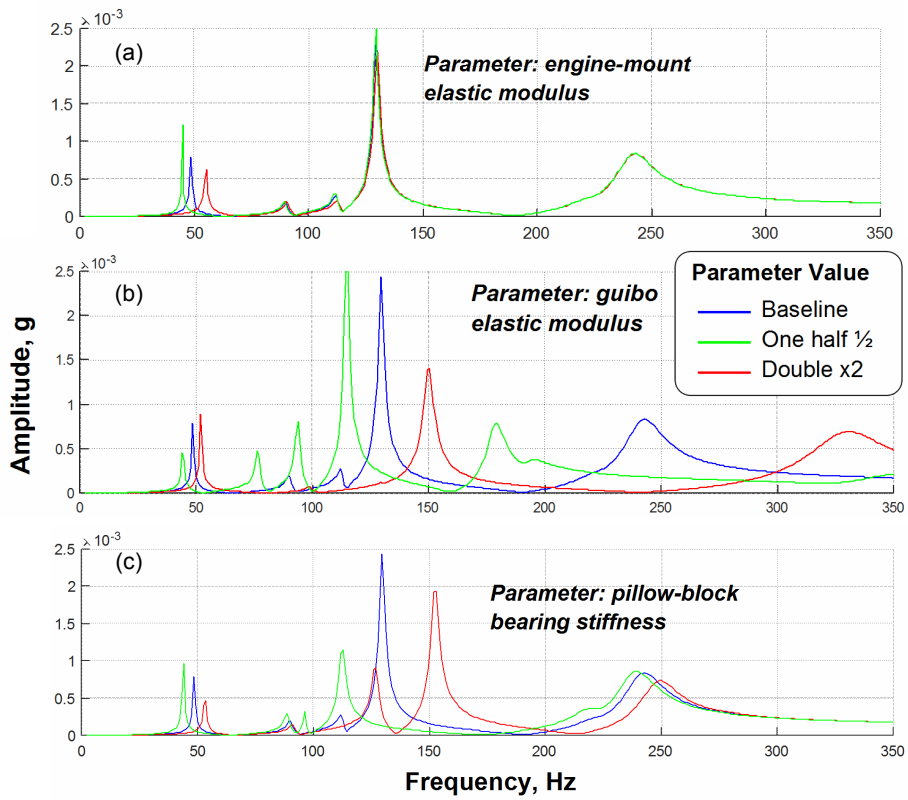

Fig. 16, Vibration frequency response comparison between rotordynamics FEM code and experimental data for SmEARF / 4 Hp engine system (engine speed 0 RPM)

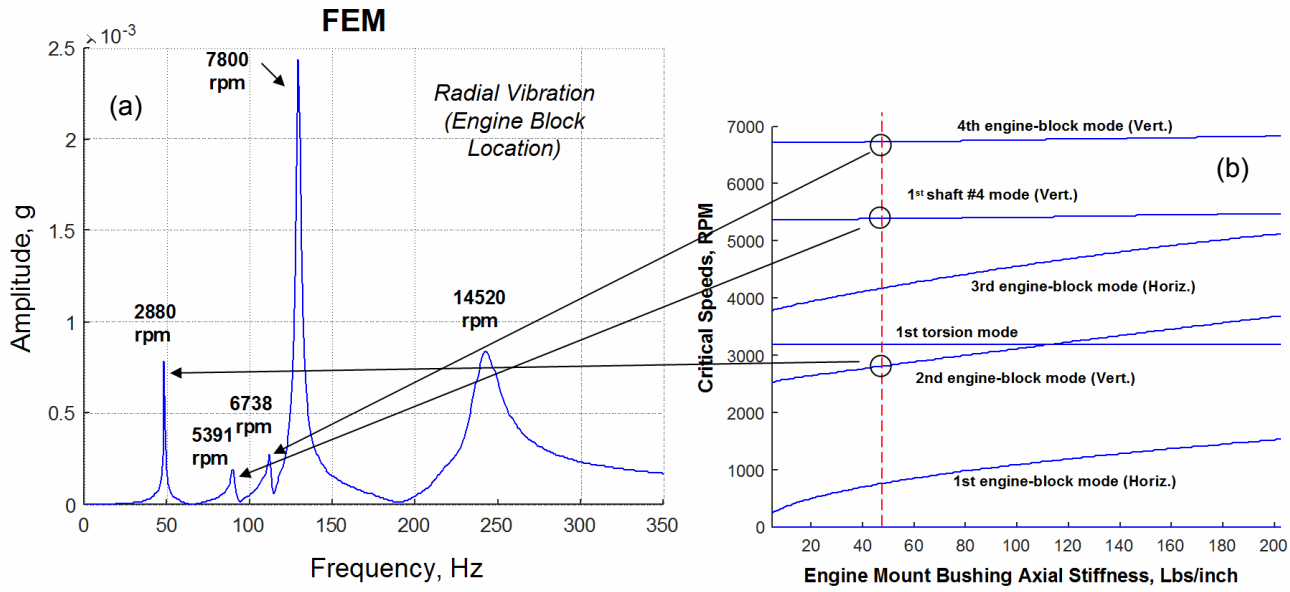

Fig. 17, Vibration frequency response comparison between rotordynamics FEM code and experimental data for SmEARF / 4 Hp engine system (engine speed 0 RPM)

Figures 16 and 17 show the strong influence of engine mount support stiffness on the system vibration response and critical speeds. Furthermore, the Campbell diagram in fig. 18 shows the effect of engine operating speed on the system natural frequencies. The 1st and 2nd lateral modes split into forward and backward whirl pairs due the engine/flywheel gyroscopic effects which become pronounced due to the relatively soft engine mounts allowing whirl to occur.

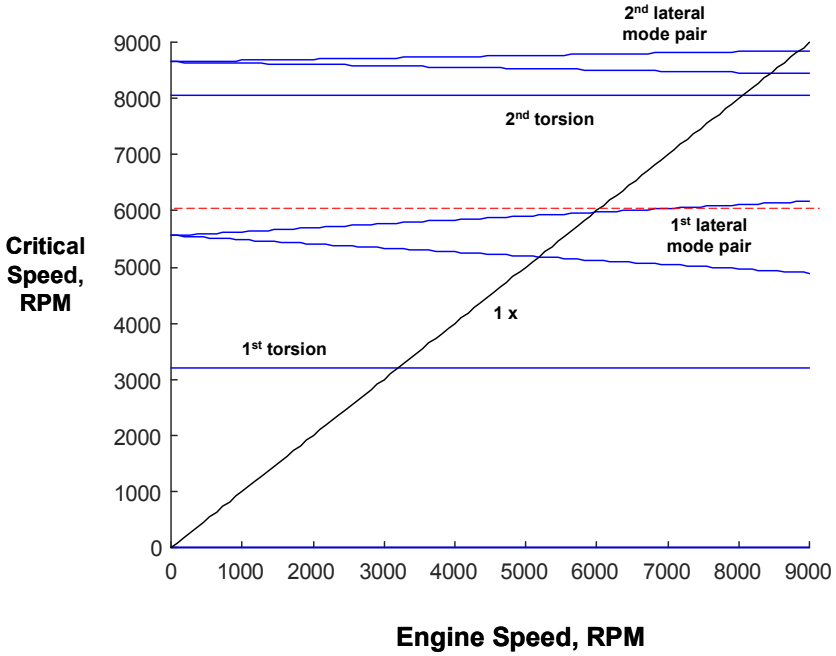

Fig. 18, Campbell Diagram: SmEARF / 4 Hp engine system critical speeds.

In addition figs. 19 - 22 summarize the rotordynamic analysis of a hybrid-electric motor / generator gearbox testrig. Specifically, fig. 19 shows a schematic diagram of the SECRL / axial flux (YASA) motor-generator hybrid electric gearbox testrig.

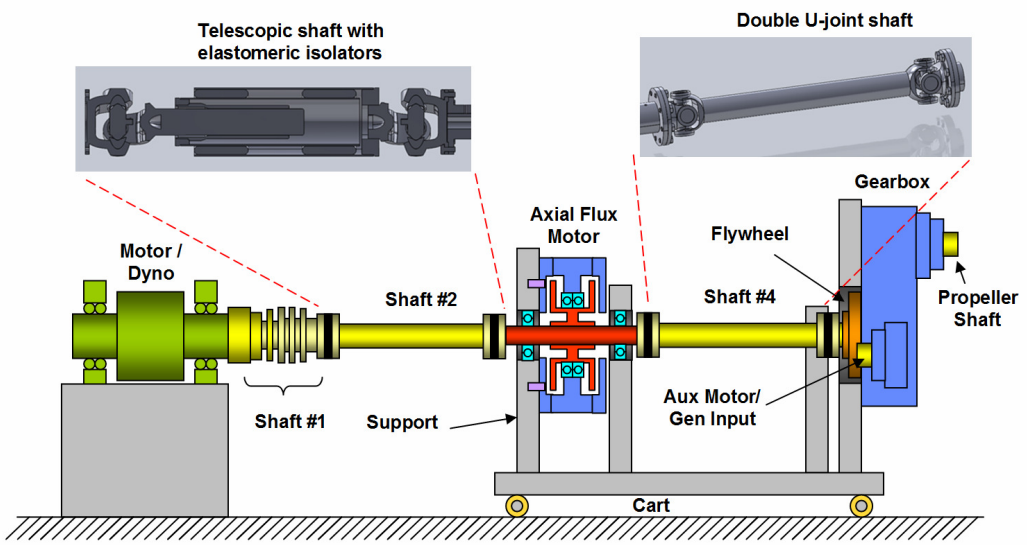

Fig. 19, Schematic diagram of SECRL / axial flux (YASA) motor-generator hybrid electric gearbox testrig

One of the key questions involved proper sizing of the center support bearings and the locations of the system critical speeds to avoid potential damage to the center axial flux (YASA) motor during shaft spinup by motor/dyno. The schematic in fig. 20 shows the implementation of the SECRL/axial flux (YASA) motor-generator gearbox testrig within the rotordynamics FEM code.

```
%%%%%%%%%%%%%%%%%%%%%%%%%%%%%%%%%%%%%%%%%%%%%%%%%%%%%%%%%%%%%%%%%%%%%%%%%%%%%%%%%%%%%%%%%%%%%%%%%%%%%%%%%%%%%%%%
%
% Dyno / Driveline / YASA / Gearbox
%                                                                 b1_yas  b2_yas
%               {n2} y-dir                                          /// ///
%                 |                     shaft "B" P/N or S/N M3390   /  /
%                 |                               ----------         \  \                       ////////
%  ///        /// |  UO G60 SD CF FA              x    s4  |         /  /                     FLY o  o
%  oo [-----] oo  |   [] [] [] [] []  []          -------  |  []    [----]    []          []  [ ][----]  {n1}
% ----[JDYNO]----[c1]-[]-[]-[]-[]-[]-[c2]--s2---==--s3--   |-[c3]---[YASA]---[c4]--------[c5]-[ ][JGBX] --->
%  oo [-----] oo      [] [] [] [] []  []          -------  |  []  / [----] /  []          []  [ ][----]  x-dir
% ///        ///                      UJ          x        |  UJ  \        \  UJ          UJ      o  o
%                          s1                     ----------      /   s6   /         s7        /////////
%                                                     s5        /////    /////
%                                                              b1_aux   b2_aux
%  Global Origin, x=O, is at Coupling [c1]
%%%%%%%%%%%%%%%%%%%%%%%%%%%%%%%%%%%%%%%%%%%%%%%%%%%%%%%%%%%%%%%%%%%%%%%%%%%%%%%%%%%%%%%%%%%%%%%%%%%%%%%%%%%%%%%%
```

Fig. 20, Rotordynamics FEM code configured for SECRL / YASA axial flux motor-generator hybrid electric gearbox testrig

One important feature not encountered in the SmEARF testrig setup described earlier is a multi-layer telescopic shaft with integrated elastomeric layers for vibration isolation.

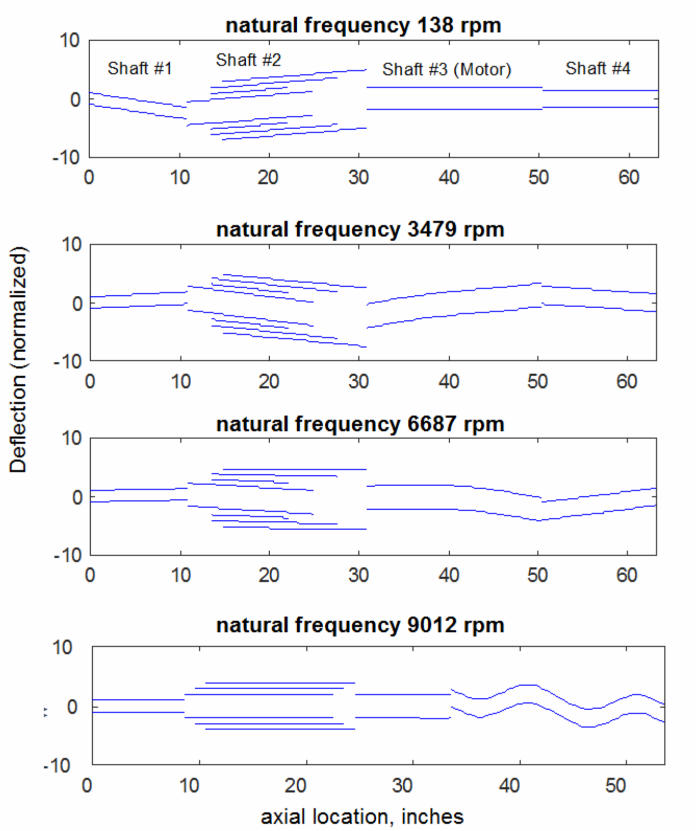

Fig. 21, 1st four lateral modeshapes of the SECRL / axial flux motor-generator hybrid electric gearbox testrig computed via the Rotordynamics FEM code (motor speed 0 RPM)

The cross-section of this telescopic shaft can be seen in fig. 19 as well as in the modeshape plots (shaft #2) in fig. 21. Figure 21 shows the 1st four lateral modeshapes and their corresponding natural frequency (in RPM).

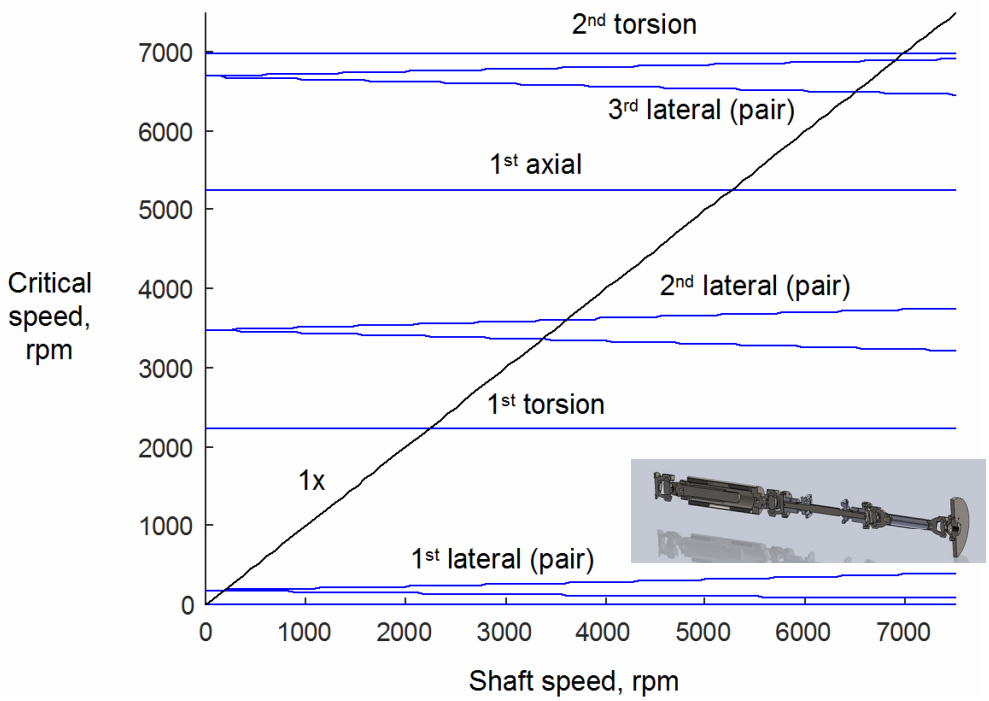

Fig. 22, Campbell Diagram: SECRL / axial flux motor-generator hybrid electric gearbox testrig critical speeds

Finally, the Campbell diagram of SECRL/axial flux motor gearbox testrig is shown in fig. 22. Here, the lateral mode natural frequency split with increasing shaft speed due to forward and backward whirl modes can be observed. This was primarily due to the gyroscopic effects of the relatively heavy multilayered shaft encounter in the initial testrig setup. Based on the predictions made by the rotordynamic FEM code, the testrig was reconfigured with a shorter lighter weight shaft which was able sufficiently move the potentially damaging lateral modes well outside of the operating speed test range.

4. Summary and Conclusions

This project developed a validated analytical model of several engine and hybrid-electric testrigs and drivelines located at Aberdeen Proving Ground to enable prediction of vibration modes and critical speeds. This effort enables more complete interpretation of experimental data as well as provides guidance for test development of different engine and hybrid-electric prototypes. Furthermore, this rotordyanmics analysis tool provides a framework in which to study hybrid electric motor/generator transient operation dynamics as well as closed-loop engine speed/fuel control interactions. The Matlab® based rotordynamic FEM code for each model has been made available to APG DEVCOM personnel. Overall this tool enhances experimental testing and validation of UAV propulsion systems and concepts.

References

1. DeSmidt, H.A., Robust-Adaptive Active Vibration Control of Alloy and Flexible Matrix Composite Rotorcraft Drivelines via Magnetic Bearings: Theory and Experiment, Ph.D. Thesis, The Pennsylvania State University, May 2005.
2. DeSmidt, H.A., Wang K.W. and Smith, E.C., ”Stability of a Segmented Supercritical Driveline with Non-Constant Velocity Couplings Subjected to Misalignment and Torque,” *Journal of Sound and Vibration*, Vol. 277, No. 4-5, pp. 895-918, 2004.